

Low-lying dipole modes in $^{26,28}\text{Ne}$ in the quasiparticle relativistic random phase approximation

Li-Gang Cao¹ and Zhong-Yu Ma^{2,*}

¹*Institute of High Energy Physics, Chinese Academy of Sciences, Beijing 100039, China*

²*China Center of Advanced Science and Technology (World Laboratory), P.O. Box 8730, Beijing 100080, China and China Institute of Atomic Energy, Beijing 102413, China*

(Received 18 July 2004; published 10 March 2005)

The low-lying isovector dipole strengths in the neutron-rich nuclei ^{26}Ne and ^{28}Ne are investigated in the quasiparticle relativistic random phase approximation. Nuclear ground-state properties are calculated in an extended relativistic mean field theory plus Bardeen-Cooper-Schrieffer (BCS) method where the contribution of the resonant continuum to pairing correlations is properly treated. Numerical calculations are tested in the case of isovector dipole and isoscalar quadrupole modes in the neutron-rich nucleus ^{22}O . It is found that in the present calculation, low-lying isovector dipole strengths at $E_x < 10$ MeV in nuclei ^{26}Ne and ^{28}Ne exhaust about 4.9% and 5.8% of the Thomas-Reiche-Kuhn dipole sum rule, respectively. The centroid energy of the low-lying dipole excitation is located at 8.3 MeV in ^{26}Ne and 7.9 MeV in ^{28}Ne .

DOI: 10.1103/PhysRevC.71.034305

PACS number(s): 21.60.Jz, 24.30.Cz, 24.30.Gd

I. INTRODUCTION

Nuclear giant resonances have been known for 50 years for the dipole mode and for more than 30 years for the other modes. But the research field was limited to excitations of nuclei along the β -stability line [1–3]. Recently, radioactive ion beam physics has become one of the frontiers in nuclear physics. It offers the possibility of broadening the study of giant resonance to weakly bound nuclei. Nuclei close to the drip line present some unique properties: a small separation energy of the valence nucleon, the smearing density distribution, and a strong coupling between the bound state and the particle continuum. These exotic properties attract more attention both experimentally and theoretically. Low-lying electric dipole modes may appear in these weakly bound nuclei, which are called pygmy dipole resonances. Although they carry only a small fraction of the full dipole strength, these states are of particular interest because they are expected to reflect the motion of the neutron skin against the core formed with an equal number of protons and neutrons. Recent experiments have shown that the increase of the dipole strength at low energies in neutron-rich nuclei could affect the corresponding radiative neutron capture cross section considerably [4], which has significance in astrophysics. Over the past decade, much experimental and theoretical effort has been dedicated to investigating properties of the low-lying dipole mode in light neutron-rich nuclei and, in particular, answering the question of whether or not these dipole excitations can be attributed to collectivity [5–16].

Recently, Beaumel *et al.* [17] have measured the inelastic scattering of $^{26}\text{Ne} + ^{208}\text{Pb}$ using a 60 MeV/u ^{26}Ne secondary beam at RIKEN. This reaction is dominated by Coulomb excitations and is selective for $E1$ transitions. The experimental

data are now under analysis [18]. In subsequent work, they will continue the experiment using a more neutron-rich projectile ^{28}Ne . Therefore, the theoretical investigation of low-lying dipole modes in ^{26}Ne and ^{28}Ne has practical significance. ^{26}Ne and ^{28}Ne are neutron-rich nuclei, whose Fermi surfaces are close to the particle continuum. Therefore, the description of these nuclei has to explicitly include the coupling between bound states and the particle continuum. The contribution of the particle continuum to the nuclear properties at low energies can mainly be attributed to a few resonant states [19–23]. On the other hand, it is well known that pairing correlations play an important role in describing properties of open shell nuclei. In order to depict the collective excitations of those nuclei, pairing correlations have to be taken into account. Recently, several theoretical works have been devoted to studying the properties of low-lying dipole modes in the framework of the quasiparticle random phase approximation (QRPA) [4,24–27]. Paar and his coworkers [28] have studied the evolution of the low-lying dipole strength in Sn isotopes in the quasiparticle relativistic random phase approximation (QRRPA) in the configuration space formalism.

In this paper, we aim to investigate the properties of low-lying dipole modes in the neutron-rich nuclei ^{26}Ne and ^{28}Ne in the QRRPA which is formulated in the response function method. The QRRPA is an extension of the fully consistent RRPAs [29–31] and takes into account the effect of pairing correlations. A consistent treatment of RRPAs within the relativistic mean field (RMF) approximation requires that the configurations include not only the pairs formed from the occupied Fermi states and unoccupied states but also the pairs formed from the Dirac states and occupied Fermi states. It has been emphasized in Refs. [29,30] that the inclusion of configurations built from positive energy states in the Fermi sea and negative energy states in the Dirac sea is essential to give an accurate quantitative description of the excitation energies of isoscalar giant multipole resonances as well as to ensure current conservation and decouple the spurious states. In the present calculations, we pay more attention to the energy-weighted moment m_1 and the centroid energy of

*Also Center of Theoretical Nuclear Physics, National Laboratory of Heavy Ion Accelerator of Lanzhou, Lanzhou 730000, and Institute of Theoretical Physics, Chinese Academy of Sciences, Beijing 100080.

the low-lying dipole strength as well as to the contribution of states around the Fermi surface to the low-lying dipole strength. Although some theoretical investigations show that ^{26}Ne and ^{28}Ne are deformed and strongly anharmonic [32–34], a spherical symmetry is assumed in the present investigation. In order to show the applicability of the method with a spherical assumption, we also study the quadrupole excitations in these nuclei and compare the calculated position and transition strength of the lowest 2^+ states with the experimental data.

In this work, the ground-state properties of the neutron-rich nuclei ^{26}Ne and ^{28}Ne are calculated in the extended relativistic mean field and the Bardeen-Cooper-Schrieffer (RMF+BCS) approximation [22], where the resonant continuum is properly treated. The empirical pairing gaps deduced from odd-even mass differences are adopted in the BCS calculation in this work. All calculations are performed with the parameter set NL3 [35], which gives a good description of not only the ground-state properties [36] but also the collective giant resonance [29–31,37–39].

The paper is arranged as follows. In Sec. II, we present the formalism of the QRRPA in the extended RMF+BCS ground state in the response function approach. In Sec. III, a test of the numerical calculation of the QRRPA in the neutron-rich nucleus ^{22}O is performed and compared with the results in Ref. [28]. In Sec. IV, the ground-state properties of ^{26}Ne and ^{28}Ne are studied in the extended RMF+BCS approach. Then the QRRPA in the response function formalism is applied to study the properties of isovector giant dipole resonances in nuclei ^{26}Ne and ^{28}Ne . Finally, we give a brief summary in Sec. V.

II. THE QUASIPARTICLE RELATIVISTIC RANDOM PHASE APPROXIMATION

There are usually two methods of obtaining the RPA strength in the study of nuclear collective excitations. One is working in a particle-hole configuration space and solving the RPA equation using a matrix diagonalization method [30]; the other is based on the linear response theory [40]. In the response function formalism, one solves a Bethe-Salpeter equation by inversion. In both methods the starting point is a self-consistent solution of the nuclear ground state. In this paper we shall work in the response function formalism and study nuclear dipole excitations in neutron-rich nuclei.

In the RRPAA calculation, we first solve the Dirac equation and equations of meson fields self-consistently in the coordinate space. The continuum is discretized by expanding nucleon spinors on a complete set basis, such as eigenfunctions in a spherical harmonic oscillator potential. Those single particle states are used to build the RRPAA configurations: a set of particle-hole pairs (ph) and pairs formed from the negative energy state in the Dirac sea and the hole state in the Fermi sea ($\bar{\alpha}h$).

The response function of a quantum system to an external field is given by the imaginary part of the polarization operator,

$$R(Q, Q; \mathbf{k}, \mathbf{k}'; E) = \frac{1}{\pi} \text{Im} \Pi^R(Q, Q; \mathbf{k}, \mathbf{k}'; E), \quad (1)$$

where Q is an external field operator. The RRPAA polarization operator is obtained by solving the Bethe-Salpeter equation:

$$\begin{aligned} \Pi(Q, Q; \mathbf{k}, \mathbf{k}', E) &= \Pi_0(Q, Q; \mathbf{k}, \mathbf{k}', E) - \sum_i g_i^2 \int d^3k_1 d^3k_2 \Pi_0 \\ &\quad \times (Q, \Gamma^i; \mathbf{k}, \mathbf{k}_1, E) D_i(\mathbf{k}_1, \mathbf{k}_2, E) \Pi(\Gamma_i, Q; \mathbf{k}_2, \mathbf{k}', E). \end{aligned} \quad (2)$$

In the RRPAA, the residual particle-hole interactions are obtained from the same Lagrangian as in the description of the nuclear ground state. They are generated by exchanging various mesons: the isoscalar scalar meson σ , the isoscalar vector meson ω , and the isovector vector meson ρ . Therefore, in Eq. (2) the sum i runs over σ, ω , and ρ mesons, and g_i and D_i are the corresponding coupling constants and meson propagators. They are $\Gamma^i = 1$ for the σ meson and $\Gamma^i = \gamma^\mu, \gamma^\mu \tau_3$ for the ω and ρ mesons, respectively. The meson propagators in the nonlinear model are nonlocal in the momentum space and therefore have to be calculated numerically. The detailed expressions of nonlinear meson propagators $D_i(\mathbf{k}_1, \mathbf{k}_2, E)$ can be found in Ref. [40]. Π_0 is the unperturbed polarization operator, which in a spectral representation has the following retarded form:

$$\begin{aligned} \Pi_0^R(P, Q; k, k'; E) &= \frac{(4\pi)^2}{2L+1} \left\{ \sum_{h,p} (-1)^{j_h+j_p} \left[\frac{\langle \bar{\phi}_h \| P_L \| \phi_p \rangle \langle \bar{\phi}_p \| Q_L \| \phi_h \rangle}{E - (\varepsilon_p - \varepsilon_h) + i\eta} \right. \right. \\ &\quad \left. \left. - \frac{\langle \bar{\phi}_p \| P_L \| \phi_h \rangle \langle \bar{\phi}_h \| Q_L \| \phi_p \rangle}{E + (\varepsilon_p - \varepsilon_h) + i\eta} \right] \right. \\ &\quad \left. + \sum_{h,\bar{\alpha}} (-1)^{j_h+j_{\bar{\alpha}}} \left[\frac{\langle \bar{\phi}_h \| P_L \| \phi_{\bar{\alpha}} \rangle \langle \bar{\phi}_{\bar{\alpha}} \| Q_L \| \phi_h \rangle}{E - (\varepsilon_{\bar{\alpha}} - \varepsilon_h) + i\eta} \right. \right. \\ &\quad \left. \left. - \frac{\langle \bar{\phi}_{\bar{\alpha}} \| P_L \| \phi_h \rangle \langle \bar{\phi}_h \| Q_L \| \phi_{\bar{\alpha}} \rangle}{E + (\varepsilon_{\bar{\alpha}} - \varepsilon_h) + i\eta} \right] \right\}. \end{aligned} \quad (3)$$

The unperturbed polarization operator includes not only the positive energy particle-hole pairs but also pairs formed from the Dirac sea states and the Fermi sea states. In Refs. [29,30] the authors show that the inclusion of configurations built from positive energy states in the Fermi sea and negative energy states in the Dirac sea is essential to give an accurate quantitative description of the excitation energies of isoscalar giant multipole resonances as well as to ensure current conservation and decouple the spurious states.

The pairing correlation and coupling to the continuum are important for exotic nuclei. A proper treatment of the resonant continuum to pairing correlations has been recently investigated in the Hartree-Fock (HF) Bogoliubov or the HF+BCS approximation [19–21] and in the extended RMF+BCS approximation [22,23]. It shows that the simple BCS approximation in the resonant continuum with a proper boundary condition works well in the description of ground-state properties even for neutron-rich nuclei. We treat the pairing correlation within the BCS approximation in this work,

and the resonant continuum is calculated by imposing an asymptotic scattering boundary condition.

When pairing correlations are taken into account, the elementary excitation is a two-quasiparticle excitation, rather than a particle-hole excitation. The unperturbed polarization operator in the QRRPA in the response function formalism can be constructed in a similar way as

$$\begin{aligned} \Pi_0^R(P, Q; k, k'; E) &= \frac{(4\pi)^2}{2L+1} \left\{ \sum_{\alpha, \beta} (-1)^{j_\alpha + j_\beta} A_{\alpha\beta} \left[\frac{\langle \bar{\phi}_\alpha \| P_L \| \phi_\beta \rangle \langle \bar{\phi}_\beta \| Q_L \| \phi_\alpha \rangle}{E - (E_\alpha + E_\beta) + i\eta} \right. \right. \\ &\quad \left. \left. - \frac{\langle \bar{\phi}_\beta \| P_L \| \phi_\alpha \rangle \langle \bar{\phi}_\alpha \| Q_L \| \phi_\beta \rangle}{E + (E_\alpha + E_\beta) + i\eta} \right] \right. \\ &\quad \left. + \sum_{\alpha, \beta} (-1)^{j_\alpha + j_\beta} v_\alpha^2 \left[\frac{\langle \bar{\phi}_\alpha \| P_L \| \phi_{\bar{\beta}} \rangle \langle \bar{\phi}_{\bar{\beta}} \| Q_L \| \phi_\alpha \rangle}{E - (E_\alpha + \lambda - \varepsilon_{\bar{\beta}}) + i\eta} \right. \right. \\ &\quad \left. \left. - \frac{\langle \bar{\phi}_{\bar{\beta}} \| P_L \| \phi_\alpha \rangle \langle \bar{\phi}_\alpha \| Q_L \| \phi_{\bar{\beta}} \rangle}{E + (E_\alpha + \lambda - \varepsilon_{\bar{\beta}}) + i\eta} \right] \right\}, \quad (4) \end{aligned}$$

with

$$A_{\alpha\beta} = (u_\alpha v_\beta + (-1)^L v_\alpha u_\beta)^2 (1 + \delta_{\alpha\beta})^{-1}, \quad (5)$$

where v_α^2 is the occupation probability, and $u_\alpha^2 = 1 - v_\alpha^2$. $E_\alpha = \sqrt{(\varepsilon_\alpha - \lambda)^2 + \Delta^2}$ is the quasiparticle energy, where λ and Δ are the Fermi energy and the pairing correlation gap, respectively. In the BCS approximation, the ϕ_α is the eigenfunction of the single-particle Hamiltonian with an eigenvalue ε_α . In Eq. (4), terms in the first square bracket represent those excitations with one quasiparticle in fully or partially occupied states and one quasiparticle in partially occupied or unoccupied states. Terms in the second square bracket describe all excitations between positive energy fully or partially occupied states and negative energy states in the Dirac sea. For unoccupied positive energy states outside the pairing active space, their energies are $E_\beta = \varepsilon_\beta - \lambda$, with occupation probabilities $v_\beta^2 = 0$ and $u_\beta^2 = 1$. For fully occupied positive energy states, the quasiparticle energy and the occupation probability are, respectively, $E_\alpha = \lambda - \varepsilon_\alpha$ and $v_\alpha^2 = 1$ in Eq. (4). States in the Dirac sea are not involved in pairing correlations. Therefore, the quantities $v_{\bar{\beta}}^2$ and $u_{\bar{\beta}}^2$ are set to be 0 and 1, respectively. Once the unperturbed polarization operator in the quasiparticle scheme is built, the QRRPA response function can be obtained by solving the Bethe-Salpeter equation (2), as is usually done in the RRPA.

III. NUMERICAL CALCULATION AND TEST OF THE QRRPA

In this section, we first check the validity of the present QRRPA calculations. We apply the QRRPA to calculate the response function of the isovector giant dipole resonance (IVGDR) and the isoscalar giant quadrupole resonance (ISGQR) in the neutron-rich nucleus ^{22}O . Similar calculations for the nucleus ^{22}O were recently performed by Paar *et al.* [28] in

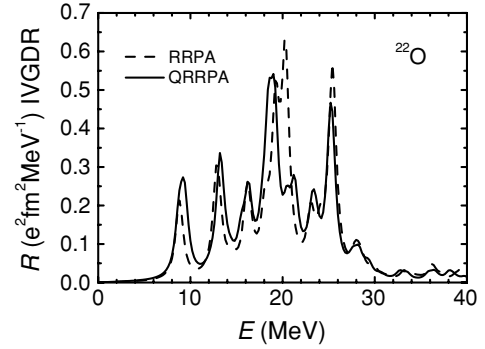


FIG. 1. IVGDR strengths in ^{22}O . The solid curve represents the result calculated in the QRRPA approach. The result calculated in the RRPA approach is shown by a dashed curve. All results are calculated with the effective Lagrangian parameter set NL3.

the framework of the relativistic Hartree-Bogoliubov (RHB) + QRRPA in the configuration space formalism.

The ground-state properties of the nucleus ^{22}O are calculated in the extended RMF+BCS approach [22] with the parameter set NL3. The neutron pairing gap is obtained from the experimental binding energies of neighboring nuclei, $\Delta_n = 1.532$ MeV. In the QRRPA calculation, particle-hole residual interactions are taken from the same effective interaction NL3, which is used in the description of the ground state of ^{22}O . Fully occupied states and states in the pairing active space are calculated self-consistently in the extended RMF+BCS approach in the coordinate space. The BCS active space is taken as all states in the sd shell as well as the $1f_{7/2}$ state, which is a resonant state in ^{22}O . A scattering boundary condition is imposed in the resonant continuum. Unoccupied states outside of the pairing active space are obtained by solving the Dirac equation in the expansion on a set of the harmonic oscillator basis. The response functions of the nuclear system to the external operator are calculated at the limit of zero momentum transfer. It is also necessary to include the space-like parts of vector mesons in the QRRPA calculations, although they do not play a role in the ground state [41]. The consistent treatment guarantees the conservation of the vector current.

In Fig. 1, we show the response function of the IVGDR mode in ^{22}O calculated in the RRPA and QRRPA approaches. The isovector dipole operator used in the calculations is [42]

$$Q = e \frac{N}{A} \sum_{i=1}^Z r_i Y_{1M}(\hat{r}_i) - e \frac{Z}{A} \sum_{i=1}^N r_i Y_{1M}(\hat{r}_i), \quad (6)$$

which excites an $L = 1$ type electric (spin-nonflip) $\Delta T = 1$ and $\Delta S = 0$ giant resonance with $J^\pi = 1^-$. The spurious state for exotic nuclei may appear at an energy of about 1 MeV in the IVGDR strength in numerical calculations due to the mixture of the isoscalar mode [43]. In our present calculations, the spurious state is removed by slightly adjusting the coupling constant of the σ meson in the residual interaction by less than 1%, which does not affect the general results.

In general, the IVGDR strengths in light stable nuclei are expected to be fragmented substantially. This also occurs in the response function of the IVGDR in neutron-rich nuclei.

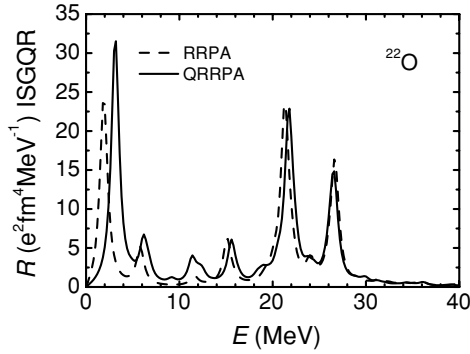


FIG. 2. ISGQR strengths in ^{22}O . Notations are the same as in Fig. 1.

More fragmented distributions around the GDR region in ^{22}O are observed in Fig. 1. In addition to the characteristic peak of the IVGDR at an energy of around 20 MeV, the low-lying dipole strength appears at an excitation energy below 10 MeV. It can be seen that the inclusion of pairing correlations enhances the low-lying dipole strength and has a slight effect on the strength at the normal dipole resonance. This illustrates the importance of including pairing correlations in the study of the low-lying isovector dipole strength in neutron-rich nuclei. The effect of pairing correlations on the isovector dipole strength in ^{22}O observed in our calculation is consistent with that obtained in the RHB+QRRPA in the configuration formalism (Fig. 2 of Ref. [28]).

The response functions of the ISGQR mode in ^{22}O calculated in the RRPA and QRRPA approaches are shown in Fig. 2. In the present calculation, the isoscalar quadrupole operator is taken from Ref. [42]:

$$Q = e \frac{Z}{A} \sum_{i=1}^A r_i^2 Y_{2M}(\hat{r}_i). \quad (7)$$

The inclusion of pairing correlations shifts the low-lying quadrupole strength to a higher energy region and enhances the low-lying quadrupole strength, whereas this only slightly affects the strength at the normal giant resonance region. A similar effect on the isoscalar quadrupole strength in ^{22}O has been observed in Fig. 3 of Ref. [28] in the framework of the RHB+QRRPA.

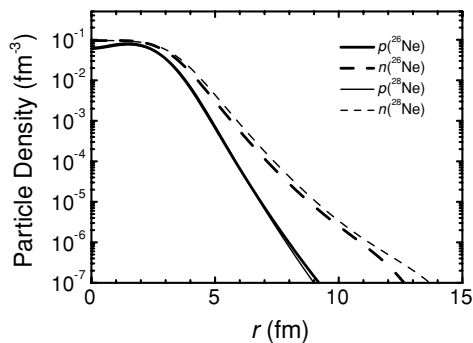


FIG. 3. Neutron and proton density distributions in nuclei ^{26}Ne and ^{28}Ne . All results are calculated in the RMF+BCS.

TABLE I. The energy-weighted moment m_1 at $E_x < 60$ MeV for the electric isovector dipole and isoscalar quadrupole excitations in ^{22}O . DC represents the result from double commutators in the nonrelativistic approach.

	DC	$m_1 (E_x < 60 \text{ MeV})$	
		RRPA	QRRPA
IVGDR($e^2 \text{ fm}^2 \text{ MeV}$)	75.9	82.08	81.71
ISGQR($e^2 \text{ fm}^4 \text{ MeV}$)	2018	1971	2159

In Table I we show the energy-weighted moment m_1 at $E_x < 60$ MeV for electric isovector dipole and isoscalar quadrupole excitations in ^{22}O . DC represents the result from double commutators in the nonrelativistic approach. In the isovector dipole mode, the value corresponds to the Thomas-Reiche-Kuhn (TRK) dipole sum rule. It is shown that the m_1 obtained by the integration of the RPA strength up to 60 MeV is slightly larger than that obtained by the double commutator (DC) in the dipole mode, whereas in the quadrupole mode, both the RRPA and QRRPA results are close to the DC value.

IV. ISOVECTOR DIPOLE EXCITATION IN THE NEUTRON-RICH NUCLEI ^{26}Ne AND ^{28}Ne

A. Ground-state properties of nuclei ^{26}Ne and ^{28}Ne

Ground-state properties of nuclei ^{26}Ne and ^{28}Ne are studied in the extended RMF+BCS with the parameter set NL3, where a spherical symmetry is assumed. The continuum is calculated by imposing a scattering boundary condition, and the width of the resonant state is not considered in this work. Constant pairing gaps are adopted in the calculation of pairing correlations, which are obtained from the experimental binding energies of neighboring nuclei by the formula

$$\Delta_p = \frac{1}{8}(B(Z-2, N) - 4B(Z-1, N) + 6B(Z, N) - 4B(Z+1, N) + B(Z+2, N)), \quad (8)$$

$$\Delta_n = \frac{1}{8}(B(Z, N-2) - 4B(Z, N-1) + 6B(Z, N) - 4B(Z, N+1) + B(Z, N+2)). \quad (9)$$

In our calculations, the neutron pairing active space in nuclei ^{26}Ne and ^{28}Ne includes states up to the $N = 28$ major shell and the $2p_{3/2}$ state, which are $1d_{5/2}$, $2s_{1/2}$, $1d_{3/2}$, $2p_{3/2}$, and $1f_{7/2}$. The BCS active space for protons is taken as all states in the sd shell. In Table II we list the neutron and proton pairing gaps in nuclei ^{26}Ne and ^{28}Ne derived from Eqs. (8) and (9) and the calculated ground-state properties, including neutron and proton Fermi energies, total binding energies, as well as the neutron and proton rms radii. The values in parentheses are corresponding experimental binding energies taken from Ref. [44]. Neutron single-particle energies and BCS occupation probabilities for those states near the neutron Fermi energy are shown in Table III, where levels ($2p_{3/2}$ and $1f_{7/2}$) with positive energies are the single-particle resonant states.

TABLE II. Neutron and proton pairing gaps in ^{26}Ne and ^{28}Ne , and calculated ground-state properties: neutron and proton Fermi energies, binding energies, as well as neutron and proton rms radii. Values in parentheses are the corresponding experimental data of the binding energy [44].

	^{26}Ne	^{28}Ne
Δ_n (MeV)	1.436	1.400
Δ_p (MeV)	2.025	2.101
λ_n (MeV)	-5.325	-4.290
λ_p (MeV)	-14.168	-16.247
E_B (MeV)	201.8(201.6)	210.5(206.9)
r_n (fm)	3.179	3.348
r_p (fm)	2.784	2.833

Thus the nucleon density with pairing correlations can be written as

$$\rho(r) = \sum_{\alpha} \frac{(2j_{\alpha} + 1)}{4\pi} v_{\alpha}^2 \phi_{\alpha}^{\dagger}(r) \phi_{\alpha}(r), \quad (10)$$

where the summation runs over all states weighted by the factor v_{α}^2 . In Fig. 3 we show the calculated nucleon densities in ^{26}Ne and ^{28}Ne . It is shown in Table II that proton rms radii are much smaller than those of neutrons. The neutron densities have far-extending tails seen in Fig. 3, which clearly shows neutron skins formed in those nuclei.

B. Low-lying isovector dipole modes in ^{26}Ne and ^{28}Ne

In this work, a spherical assumption is adopted in the RMF and RRP A calculation, although ^{26}Ne and ^{28}Ne are deformed and anharmonic. In order to see to what extent the present model can be effective, one first studies the quadrupole excitations in these nuclei and compares them with the experimental data. The calculated energies and $B(E2)$ values for the lowest 2^+ states in ^{26}Ne and ^{28}Ne are listed in Table IV. The values in parentheses are the corresponding experimental data taken from Ref. [45]. Although the $B(E2)$ value in ^{28}Ne is very close to the lower limit of the experimental data, the present calculations reasonably reproduce the lowest 2^+ states and their $B(E2)$ values.

We now apply the QRRPA approach to investigate the isovector dipole response in ^{26}Ne and ^{28}Ne . We focus our attention on properties of the isovector low-lying dipole

TABLE III. Neutron single particle energies ε_{α} and occupation probabilities v_{α}^2 of levels near the neutron Fermi energy in nuclei ^{26}Ne and ^{28}Ne .

	^{26}Ne		^{28}Ne	
	ε_{α} (MeV)	v_{α}^2	ε_{α} (MeV)	v_{α}^2
$1d_{5/2}$	-10.548	0.982	-10.836	0.989
$2s_{1/2}$	-6.549	0.824	-7.054	0.946
$1d_{3/2}$	-3.408	0.099	-4.299	0.503
$2p_{3/2}$			0.786	0.018
$1f_{7/2}$	2.946	0.007	2.223	0.011

TABLE IV. The calculated energies and $B(E2)$ values for the lowest 2^+ states in ^{26}Ne and ^{28}Ne . The values in parentheses are the corresponding experimental data taken from Ref. [45].

	E_{2^+} (MeV)	$B(E2)$ ($e^2 \text{fm}^4$)
^{26}Ne	1.46(1.99 \pm 0.012)	223(228 \pm 41)
^{28}Ne	1.29(1.32 \pm 0.020)	156(269 \pm 136)

strength. In Fig. 4, we present the Hartree and perturbed strengths for the isovector dipole mode in nuclei ^{26}Ne (upper panel) and ^{28}Ne (lower panel) calculated in the RRP A and QRRPA approaches. Short-dashed curves represent the RRP A strengths; the QRRPA response functions are denoted by solid curves. In Fig. 4, it can be seen that the perturbed strengths at energies above 10 MeV for these neutron-rich nuclei are very fragmented. Compared to the Hartree strengths, the RPA strengths are shifted to a higher energy region due to the repulsive particle-hole residual interaction generated mainly by exchanging a ρ meson.

In addition to the characteristic peak of the IVGDR around an energy of 20 MeV, low-lying dipole strengths appear at excitation energy below 10 MeV. It is shown in Fig. 4 that the effect of pairing correlations on the isovector dipole strength in ^{26}Ne and ^{28}Ne is to shift the low-lying dipole strength to a higher energy region and decrease the low-lying dipole strength, especially in ^{26}Ne . The situation slightly differs from that in ^{22}O , where the low-lying strength is increased. The decrease of the low-lying strength is mainly due to the fact that two-quasiparticle excitations in the dipole mode are weakened

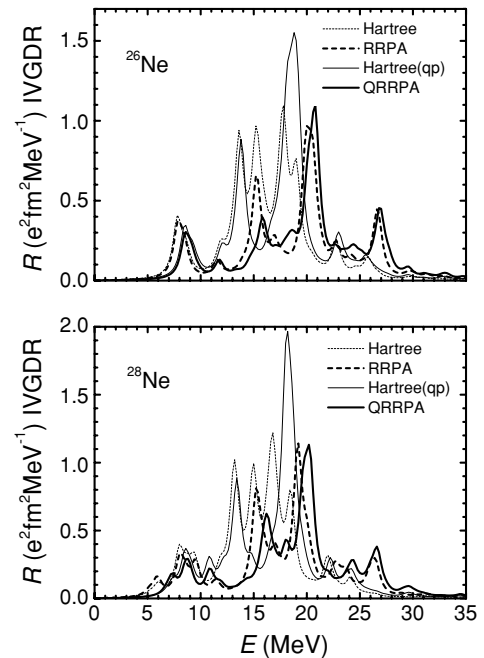


FIG. 4. Isovector dipole strength functions in neutron-rich nuclei ^{26}Ne (upper panel) and ^{28}Ne (lower panel). The QRRPA responses with the pairing (solid curves) are compared with the RRP A calculation without the pairing (dashed curves). The thick and thin curves represent perturbed and Hartree strengths, respectively.

by a factor of v_α^2 when the pairing correlation is switched on. In addition, the two-quasiparticle excitation energy is larger than the corresponding particle-hole excitation energy in the dipole mode [27]. On the contrary, when the pairing correlation is taken into account the configuration space becomes larger, which allows for the particle-particle and hole-hole transitions. This enlarged configuration space may increase the low-lying strength. As analyzed below, the state $2s_{1/2}$ produces a large contribution to the low-lying strength of the dipole mode in $^{26,28}\text{Ne}$ and ^{22}O . It is known that the $2s_{1/2}$ state is located below and above the Fermi surface in $^{26,28}\text{Ne}$ and ^{22}O , respectively. Therefore, particle-particle excitations, especially due to the particle state $2s_{1/2}$, largely enhance the low-lying strength in ^{22}O , which is not true in the case of ^{26}Ne and ^{28}Ne .

In comparison with the Hartree strength, it is found that the RPA strength of the isovector dipole mode at the low-energy region in ^{26}Ne and ^{28}Ne shown in Fig. 4 remains at its position and is created mainly from a few particle-hole configurations, which show that it has a single-particle-like property. The low-lying strength is slightly attracted back to the lower energy, which is due to the correlations of the isoscalar operator in the isovector mode [43]. Differing from the normal IVGDR response, the low-lying resonance can be interpreted as the excitation of the excess neutrons out of phase with the core formed with an equal number of protons and neutrons [14]. Analyzing the Hartree strength of the isovector dipole mode in ^{26}Ne at energies below 10 MeV calculated with pairing correlations, one finds a pronounced peak around 8.5 MeV, which is formed mainly from the neutron configurations of $\nu(2s_{1/2}^{-1}2p_{3/2})$ (8.482 MeV) and $\nu(2s_{1/2}^{-1}2p_{1/2})$ (9.232 MeV), where the values in parentheses are their Hartree energies. Since 16 neutrons in ^{26}Ne fill neutron orbits up to $2s_{1/2}$ and form a subclosed shell, the occupation probabilities at $1d_{3/2}$ and $1f_{7/2}$ states in ^{26}Ne are relatively small (see Table III). Therefore, the contribution from neutron states $1d_{3/2}$ and $1f_{7/2}$ to the low-lying Hartree strength is insignificant. In contrast, for the Hartree strength at the low energy region in ^{28}Ne , in addition to the peaks formed from the neutron configurations of $\nu(2s_{1/2}^{-1}2p_{3/2})$ (8.523 MeV) and $\nu(2s_{1/2}^{-1}2p_{1/2})$ (9.080 MeV), a few more peaks appear, which are formed from the neutron excitation between the bound level $1d_{3/2}$ and levels in the continuum. It is found that the Hartree strengths at the low-lying dipole in ^{26}Ne and ^{28}Ne are mainly due to neutron excitations near the Fermi surface.

Although the Hartree low-lying strength is mainly formed from the neutron excitations, the RPA strengths are fully

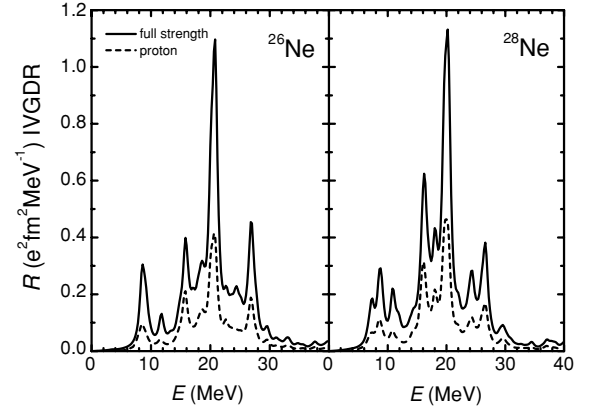


FIG. 5. The contribution of the proton to the isovector dipole strengths in ^{26}Ne (left panel) and ^{28}Ne (right panel) in the QRRPA approach. The solid curves are the full QRRPA strengths. The dashed curves represent strengths from the proton.

correlated and contributed from both neutron and proton. To illustrate the contribution of the proton to the full strength, we set a very small value of the neutron effective charge in the dipole operator instead of eZ/A . Results are plotted in Fig. 5. The dashed curves represent the strengths from the proton, which are compared with the full QRRPA strengths denoted by solid curves. Figure 5 clearly shows that the proton also plays an important role in the perturbed strength at low-lying dipole states.

In Ref. [14], the authors have studied the evolution of collectivity in the isovector dipole response in the low-lying region for neutron-rich isotopes of O, Ca, Ni, Zr, and Sn using the RRPA method. They conclude that in light neutron-rich nuclei, such as neutron-rich isotopes of O and Ca, the onset of dipole strength in the low-lying region is due to single particle excitations of the loosely bound neutrons. By analyzing the structure of RRPA strengths in a low-lying region in nuclei ^{26}Ne and ^{28}Ne , we find that there are only several configurations contributing to the low-lying RRPA strength, and the RRPA strengths remain in their positions compared to the Hartree strengths in the low-energy region, which mean that the RRPA strengths in the low-lying region in nuclei ^{26}Ne and ^{28}Ne are dominated by single particle transitions.

In order to give a clearer description of those isovector low-lying dipole states obtained in the QRRPA approach, we calculate various moments of isovector dipole strengths at a

TABLE V. The non-energy-weighted moment m_0 and the energy-weighted moment m_1 of isovector dipole strengths in ^{26}Ne and ^{28}Ne in the QRRPA calculations. We separate the energy region into low energies ($0 \text{ MeV} \leq E_x \leq 10 \text{ MeV}$) and high energies ($10 \text{ MeV} \leq E_x \leq 30 \text{ MeV}$). The values in the last two columns are obtained from the classical TRK dipole sum rule and the TRK cluster sum rule ($e^2 \text{ fm}^2 \text{ MeV}$). The units are $e^2 \text{ fm}^2$ and $e^2 \text{ fm}^2 \text{ MeV}$ for m_0 and m_1 , respectively.

	$0 \text{ MeV} \leq E_x \leq 10 \text{ MeV}$		$10 \text{ MeV} \leq E_x \leq 30 \text{ MeV}$		S_{TRK}	S_{Clus}
	m_0	m_1	m_0	m_1		
^{26}Ne	0.542	4.525	5.032	103.9	91.7	17.2
^{28}Ne	0.705	5.606	5.648	111.2	95.8	21.3

given energy interval

$$m_k = \int_{E_1}^{E_2} R^L(E) E^k dE, \quad (11)$$

where E_1 and E_2 are the lower and upper energies of the integral, respectively. The RPA equation is solved until $E = 60$ MeV in the present calculations. The non-energy-weighted moment m_0 and the energy-weighted moment m_1 of isovector dipole strengths in ^{26}Ne and ^{28}Ne are calculated at two energy intervals: the low-energy region ($0 \text{ MeV} \leq E_x \leq 10 \text{ MeV}$) and the high-energy region ($10 \text{ MeV} \leq E_x \leq 30 \text{ MeV}$), which are listed in Table IV. The values obtained from the Thomas-Reiche-Kuhn (TRK) dipole sum rule are listed in the sixth column. In our present QRRPA calculations, the low-lying isovector dipole strengths in ^{26}Ne and ^{28}Ne exhaust about 4.93% and 5.85% of the TRK dipole sum rule, respectively. This is consistent with recent experimental observations in ^{18}O , ^{20}O , and ^{22}O , where the low-lying isovector dipole strengths exhaust about 5% of the TRK dipole sum rule [13]. In general, the percentage of the low-lying isovector dipole strength becomes larger as the neutron excess increases [14]. The energy-weighted moment m_1 at $E_x < 10$ MeV in ^{28}Ne is about 1.0% larger than that in ^{26}Ne .

On the other hand, the cluster sum rule [7,8,46,47] is usually used to understand the properties of low-lying dipole strength in exotic nucleus excitations. Here, we choose ^{20}Ne as the core. In Table V, we also list the values obtained from the TRK cluster dipole sum rule, say, $17.2 e^2 \text{ fm}^2 \text{ MeV}$ and $21.3 e^2 \text{ fm}^2 \text{ MeV}$ for ^{26}Ne and ^{28}Ne , respectively. Table V shows that the low-lying dipole excitations in these two neutron-rich nuclei exhaust about 26.3% of the TRK cluster dipole sum rule. Similar results are obtained in Ref. [7] for neutron-rich isotopes.

The centroid energy of the response function is defined as

$$\bar{E} = m_1/m_0. \quad (12)$$

We separate the energy interval into two regions: $0 \text{ MeV} < E_x < 10 \text{ MeV}$ and $10 \text{ MeV} < E_x < 60 \text{ MeV}$. The centroid energies in these two energy regions are listed in Table VI. In the QRRPA calculations, the centroid energies of low-lying isovector dipole strengths in ^{26}Ne and ^{28}Ne are 8.34 and 7.94 MeV, respectively, whereas the centroid energies of the

TABLE VI. Centroid energies of the isovector dipole response functions in ^{26}Ne and ^{28}Ne . The centroid energies are calculated within $0 \sim 10$ and $10 \sim 60$ MeV, respectively. All energy values are in units of MeV.

	^{26}Ne	^{28}Ne
$\bar{E}(0 \sim 10)$	8.34	7.94
$\bar{E}(10 \sim 60)$	22.32	21.13

normal IVGDR strengths are located at 22.3 MeV for ^{26}Ne and 21.1 MeV for ^{28}Ne .

V. SUMMARY

In this paper we have studied the properties of low-lying isovector dipole resonances in the neutron-rich nuclei ^{26}Ne and ^{28}Ne in the framework of the QRRPA with the effective Lagrangian parameter set NL3. The ground-state properties are calculated in the extended RMF+BCS approach, where the resonant continuum is properly treated. Constant pairing gaps extracted from the experimental binding energies of neighboring nuclei are adopted in the BCS calculation. In the QRRPA calculation, the negative energy states in the Dirac sea are included for completeness. It is shown that the inclusion of pairing correlations has a relatively strong effect on the low-lying isovector dipole strength in neutron-rich nuclei. In the QRRPA calculation, the low-lying isovector dipole strengths in ^{26}Ne and ^{28}Ne exhaust about 5% and 26.3% of the TRK dipole sum rule and the TRK dipole cluster sum rule, respectively. The centroid energies of the low-lying dipole excitation in nuclei ^{26}Ne and ^{28}Ne are located around 8.0 MeV.

ACKNOWLEDGMENTS

We thank Professor Didier Beaumel, Nguyen Van Giai, Zong-ye Zhang, and You-wen Yu for many useful discussions. This work is supported by the National Natural Science Foundation of China under Grant Nos. 10305014, 90103020, and 10275094, and by the Major State Basic Research Development Program in China under Contract No. G2000077400.

-
- [1] B. L. Berman and S. C. Fultz, *Rev. Mod. Phys.* **47**, 713 (1975).
[2] J. Speth, *Electric and Magnetic Giant Resonances in Nuclei* (World Scientific, Singapore, 1991).
[3] R. Pitthan and Th. Walcher, *Phys. Lett.* **B36**, 563 (1971).
[4] S. Goriely and E. Khan, *Nucl. Phys.* **A706**, 217 (2002).
[5] E. Tryggestad *et al.*, *Phys. Rev. C* **67**, 064309 (2003).
[6] N. Ryezayeva *et al.*, *Phys. Rev. Lett.* **89**, 272502 (2002).
[7] A. Leistenschneider *et al.*, *Phys. Rev. Lett.* **86**, 5442 (2001).
[8] T. Aumann *et al.*, *Phys. Rev. C* **59**, 1252 (1999).
[9] Y. Iwata *et al.*, *Phys. Rev. C* **62**, 064311 (2000).
[10] H. Iwasaki *et al.*, *Phys. Lett.* **B491**, 8 (2000).
[11] D. Sackett *et al.*, *Phys. Rev. C* **48**, 118 (1993).
[12] T. Nakamura *et al.*, *Phys. Lett.* **B331**, 296 (1994).
[13] T. Aumann *et al.*, *Nucl. Phys.* **A649**, 297c (1996).
[14] D. Vretenar, N. Paar, P. Ring, and G. A. Lalazissis, *Nucl. Phys.* **A692**, 496 (2001).
[15] H. Sagawa, T. Suzuki, H. Iwasaki, and M. Ishihara, *Phys. Rev. C* **63**, 034310 (2001).
[16] H. Sagawa and T. Suzuki, *Phys. Rev. C* **59**, 3116 (1999).
[17] D. Beaumel (private communication).
[18] J. Gibelin *et al.*, *RIKEN Accel. Prog. Rep.* **37**, 1 (2004).

- [19] N. Sandulescu, N. V. Giai, and R. J. Liotta, Phys. Rev. C **61**, 061301 (2000).
- [20] A. T. Kruppa, P. H. Heenen, and R. J. Liotta, Phys. Rev. C **63**, 044324 (2001).
- [21] M. Grasso, N. Sandulescu, N. V. Giai, and R. J. Liotta, Phys. Rev. C **64**, 064321 (2001).
- [22] Li-Gang Cao and Zhong-Yu Ma, Eur. Phys. J. A **22**, 189 (2004).
- [23] N. Sandulescu, L. S. Geng, H. Toki, and G. C. Hillhouse, Phys. Rev. C **68**, 054323 (2003).
- [24] S. Kamedzhiev, R. J. Liotta, E. Litvinova, and V. Tselyaev, Phys. Rev. C **58**, 172 (1998).
- [25] E. Khan and N. V. Giai, Phys. Lett. **B472**, 253 (2000).
- [26] Masayuki Matsuo, Nucl. Phys. **A696**, 371 (2001).
- [27] K. Hagino and H. Sagawa, Nucl. Phys. **A695**, 82 (2001).
- [28] N. Paar, P. Ring, T. Niksic, and D. Vretenar, Phys. Rev. C **67**, 034312 (2003).
- [29] Zhong-Yu Ma, N. V. Giai, A. Wandelt, D. Vretenar, and P. Ring, Nucl. Phys. **A686**, 173 (2001); Zhong-Yu Ma, Comm. Theor. Phys. **32**, 493 (1999).
- [30] P. Ring, Zhong-Yu Ma, N. V. Giai, A. Wandelt, D. Vretenar, and Li-Gang Cao, Nucl. Phys. **A694**, 249 (2001).
- [31] Zhong-Yu Ma, A. Wandelt, N. V. Giai, D. Vretenar, P. Ring, and Li-Gang Cao, Nucl. Phys. **A703**, 222 (2002).
- [32] Y. Utsuno, T. Otsuka, T. Mizusaki, and M. Honma, Phys. Rev. C **60**, 054315 (1999).
- [33] P.-G. Reinhard, D. J. Dean, W. Nazarewicz, J. Dobaczewski, J. A. Maruhn, and M. R. Strayer, Phys. Rev. C **60**, 014316 (1999).
- [34] F. Azaiez, Nucl. Phys. **A704**, 37c (2002).
- [35] G. A. Lalazissis, J. König, and P. Ring, Phys. Rev. C **55**, 540 (1997).
- [36] G. A. Lalazissis, S. Raman, and P. Ring, At. Data Nucl. Data Tables **71**, 1 (1999).
- [37] D. Vretenar, A. Wandelt, and P. Ring, Phys. Lett. **B487**, 334 (2000).
- [38] Li-Gang Cao and Zhong-Yu Ma, Phys. Rev. C **66**, 024311 (2002).
- [39] Li-Gang Cao and Zhong-Yu Ma, Chin. Phys. Lett. **20**, 1459 (2003).
- [40] Zhong-Yu Ma, H. Toki, N. V. Giai, Nucl. Phys. **A627**, 1 (1997).
- [41] P. Ring, Prog. Part. Nucl. Phys. **37**, 197 (1996).
- [42] K. F. Liu, Hongde Luo, and Zhong-Yu Ma, Nucl. Phys. **A534**, 25 (1991).
- [43] Li-Gang Cao, Bao-Qiu Chen, and Zhong-Yu Ma, Comm. Theor. Phys. **36**, 178 (2001).
- [44] G. Audi and A. H. Wapstra, Nucl. Phys. **A595**, 409 (1995).
- [45] B. V. Pritychenko *et al.*, Phys. Lett. **B461**, 322 (1999).
- [46] Y. Alhassid, M. Gai, and G. F. Bertsch, Phys. Rev. Lett. **49**, 1482 (1982).
- [47] K. Hencken, G. Baur, and D. Trautmann, Nucl. Phys. **A733**, 200 (2004).